

SCIENTIFIC REPORTS



OPEN

Posing for a picture: vesicle immobilization in agarose gel

Rafael B. Lira^{1,2}, Jan Steinkühler², Roland L. Knorr², Rumiana Dimova² & Karin A. Riske¹

Received: 12 January 2016

Accepted: 13 April 2016

Published: 03 May 2016

Taking a photo typically requires the object of interest to stand still. In science, imaging is potentiated by optical and electron microscopy. However, living and soft matter are not still. Thus, biological preparations for microscopy usually include a fixation step. Similarly, immobilization strategies are required for or substantially facilitate imaging of cells or lipid vesicles, and even more so for acquiring high-quality data via fluorescence-based techniques. Here, we describe a simple yet efficient method to immobilize objects such as lipid vesicles with sizes between 0.1 and 100 μm using agarose gel. We show that while large and giant unilamellar vesicles (LUVs and GUVs) can be caged in the pockets of the gel meshwork, small molecules, proteins and micelles remain free to diffuse through the gel and interact with membranes as in agarose-free solutions, and complex biochemical reactions involving several proteins can proceed in the gel. At the same time, immobilization in agarose has no adverse effect on the GUV size and stability. By applying techniques such as FRAP and FCS, we show that the lateral diffusion of lipids is not affected by the gel. Finally, our immobilization strategy allows capturing high-resolution 3D images of GUVs.

Microscopy imaging of cellular and model membranes has revealed a wealth of information about membrane structure and properties. As such, examples include measurements of diffusion coefficient of lipids¹ and membrane proteins², imaging of membrane domains³, and extraction of mechanical information⁴ *in vitro* and *in vivo*. Due to the complex nature and dynamics of living cells, these parameters are commonly studied on model membrane systems, in which the properties are easily controlled by the appropriate choice of their components. Such models include lipid monolayers, supported and black lipid bilayers, lipid-based emulsions, small and large unilamellar vesicles (SUVs and LUVs, respectively) and giant unilamellar vesicles (GUVs). The advantage of vesicles is that they are free-standing closed lipid bilayers with minimal or no contact to the support, no presence of residuals from their preparation, and they represent a very good reporter of membrane properties.

SUVs and LUVs, to which we will refer from now on as liposomes, are classical membrane models with straightforward preparation and characterization. Bulk experiments performed with populations of liposomes are inherently limited to the sampling of the whole population and the obtained results are averaged out over individual inhomogeneities. Yet, single-liposome assays are becoming increasingly popular^{5–7}. On the other hand, cell-sized GUVs are observed and manipulated under the microscope as single objects and GUV imaging and manipulation have allowed the investigation of a wide range of membrane and vesicle properties^{8–10}, which is otherwise very difficult or impossible to accomplish with small liposomes.

Many fluorescence-based measurements performed on the membrane require it to be immobile during sampling. This is the case of quantitative fluorescence techniques such as fluorescence recovery after photobleaching (FRAP) and fluorescence correlation spectroscopy (FCS), in which the examined region of interest (ROI) must be fixed during the measurement. An immobilized sample would also facilitate other imaging techniques, including fluorescence lifetime microscopy (FLIM) and three-dimensional reconstruction of GUVs with confocal microscopy as well as with super-resolution microscopy techniques. Very often, 3D imaging is limited to one vesicle half (rather than the whole vesicle surface) due to time constraints. The obtained images are often distorted or blurry due to small movements of the vesicle. Lateral displacements may lead to artifacts and, hence, result in data which are either useless or difficult to interpret.

Despite the need, only a few studies have attempted establishing vesicle immobilization. GUVs and liposomes can be immobilized at a functionalized surface through specific biotin-avidin binding¹¹, but this approach leads to changes in composition of the adhering area^{12,13}. Another possibility is to apply a magnetic or electric field to trap the vesicles¹⁴, but in this case, tension is imposed on the membrane. Optical traps or stretchers can also be

¹Departamento de Biofísica, Universidade Federal de São Paulo, São Paulo, Brazil. ²Department of Theory and Bio-Systems, Max Planck Institute of Colloids and Interfaces, Potsdam, Germany. Correspondence and requests for materials should be addressed to R.D. (email: dimova@mpikg.mpg.de) or K.A.R. (email: kariske@unifesp.br)

employed, but one either needs a handle in the form of a particle attached to the membrane or else local heating may occur¹⁵, and both setups require sophisticated equipment. The latter applies also to vesicle trapping in microfluidic devices¹⁶. Alternatively, GUVs prepared on electrode wires remain attached to the electrodes¹⁷ but the vesicle is not isolated and typically connected by a thin tether to the electrode. An interesting option is to arrest vesicles inside a mesh of polymerizable molecules. Esquembre *et al.* reported efficient GUV immobilization on a mesh of porous silica glasses¹⁸. However, all measured parameters such as lipid order and molecular mobility were significantly altered by the support and larger GUVs were observed to collapse. In a similar approach, hydrogels were used to immobilize proteo-GUVs¹⁹, but protein activity was shown to be reduced upon immobilization. Similarly, Tsumoto *et al.* used relatively high agarose concentrations to study morphological and permeability changes induced on embedded GUVs by adding membrane-active molecules²⁰, but no detailed characterization of possible immobilization effects was shown.

In this work, we report a functional, efficient and simple vesicle immobilization method based on the thermal properties of agarose polymers. The vesicles were dispersed in fluid agarose, above the polymer melting temperature, and became readily immobilized when the dispersion cooled down to room temperature and agarose became a gel. The immobilization method proposed here is simple and fast to implement, does not require any special equipment, expensive chemicals or expertise in microfluidics design, and is potentially applicable in any laboratory.

Results

Extracting quantitative information from experiments with GUVs is often challenging. In many applications, it is crucial that the GUVs remain immobile throughout the sampling time, which may span up to minutes. In a typical experiment, GUVs are dispersed in aqueous solutions and diffusive motion and convective flows lead to vesicle drift inside the observation chamber. These movements preclude or at best make these measurements difficult. To expand the range of routine biophysical applications of GUVs, we envisaged a simple albeit efficient immobilization method, based on the presence of agarose gel in the external vesicle solution.

Low-melting temperature agarose polymer ($T_m \sim 62^\circ\text{C}$, $T_g \sim 26^\circ\text{C}$) was used to immobilize GUVs and liposomes. Agarose forms a gel at room temperature and is fluid at temperatures above the melting temperature T_m . It exhibits large hysteresis, becoming a gel again when the temperature is decreased below the gelation temperature T_g . Vesicles and agarose were mixed while the polymer was still in the fluid state (around $35\text{--}40^\circ\text{C}$) at 0.5% w/v agarose concentration if not mentioned otherwise. This concentration was chosen based on the best balance between immobilization efficiency and undesired morphological deformations (see below). After mixing, the sample was left for at least ten minutes at room temperature for agarose jellification. Interacting molecules were added to the sample before or after polymer jellification as further indicated for the given experiment (see sketch of the observation chamber in Fig. S1).

GUVs are fully immobilized but unperturbed by the agarose gel. In a typical experiment and without any immobilization strategy (e.g., fixing or tethering to a surface or by means of optical trapping, micropipette manipulation or microfluidic posts), GUVs display micrometer-length lateral displacement during typical observation times (from several seconds to a few minutes). The drifting becomes even more pronounced in the presence of convective flows ensuing from the assembly of the observation chamber. An example of such GUV displacement is shown in Fig. 1A (upper-left image), in which consecutive snapshots of a free GUV taken every 5 s are overlaid in one image. In large contrast, when dispersed in 0.5% w/v agarose gel, vesicles are fully immobilized, displaying no visible lateral displacement at least within 10 min (Fig. 1A, upper-right image). Importantly, thermal shape fluctuations are not suppressed (see movie in the Supplementary Information), although possibly reduced. At low concentrations of agarose (up to 0.1% w/v), vesicles are still able to move, although much more slowly (a few $\mu\text{m}/\text{min}$), whereas at concentrations of 0.25–0.5% w/v agarose or higher, their lateral displacement is completely suppressed (see Fig. 1A). At high agarose concentrations (1% w/v agarose), deformed GUVs and GUVs with long and externally protruding lipid tubes were often observed (Fig. S2).

Immobilization efficiency was examined not only for the equatorial cross sections but also at the vesicle poles, since many fluorescence-based applications, such as FRAP and FCS, require observation of a selected membrane area (region of interest, ROI) imaged for long times. Figure 1A, lower-left image, shows overlay images of the upper pole of a non-immobilized GUV during the measurement time (45 s). The vesicle clearly displayed a drift. In contrast, immobilization efficiently preserves the vesicle position for at least several minutes (Fig. 1A, lower-right image). In both cases, ROIs (white circles with radii proportional to the GUV sizes) were selected at the GUV pole in the first imaging frame. Membrane fluorescence intensities within the ROIs (normalized to the first frames) are shown as a function of time in Fig. 1B for both cases. Whereas the fluorescence intensity remains constant for the immobilized vesicle (red data points), it varies significantly when the non-immobilized vesicle drifts during the measurement (black data points). This result demonstrates the efficiency of the immobilization method for performing quantitative measurements both at the GUV equator and the poles.

One of the obvious benefits of the immobilization strategy is to obtain high-resolution 3D images of GUVs. Such image reconstructions allow complete representation of the vesicle topology and are particularly important for imaging GUVs exhibiting phase separation. Figure 1C shows detailed reconstructed images of two GUVs immobilized in agarose. The image on the left shows a vesicle composed of DOPG:SM:chol (3:5:2–molar ratio) exhibiting Lo/Ld (liquid-ordered/liquid-disordered) phase separation. The image is a whole-vesicle 3D projection reconstructed from 262 slices. The acquisition took over 5 minutes, which would be very difficult to achieve with freely suspended GUVs. Domains as well as their shapes are clearly seen in the image, which contains no blurriness whatsoever. The image on the right in Fig. 1C was obtained from the upper hemisphere of a GUV made of SM, which exhibits facets characteristic of the gel phase. The surface topology can be clearly seen. Images with higher resolution demanding even longer sampling times could also be obtained.

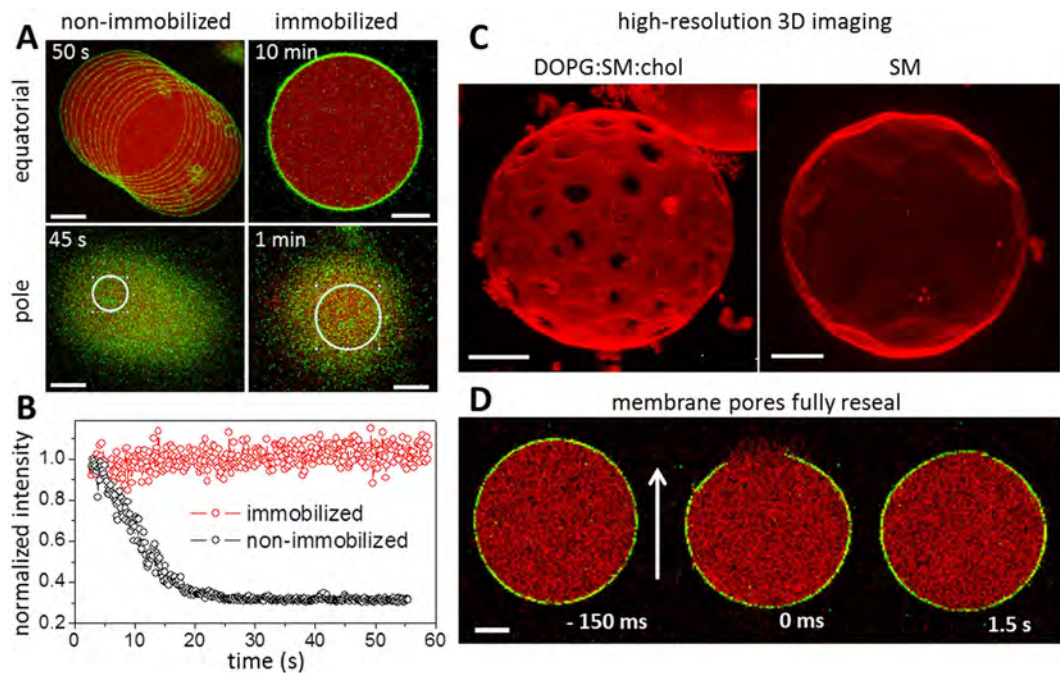


Figure 1. GUV immobilization efficiency. (A) Overlay of consecutive snapshots of POPC GUVs in the absence (left) and presence (right) of 0.5% w/v agarose gel in the external medium. Upper and lower images show confocal images of the equatorial cross sections (top) and the vesicle surface at the poles (bottom), respectively. The total measurement time is shown in the top corner of each picture. The membrane is labeled with 0.5 mol% of NBD-PE (false green color) and the vesicles encapsulate 2.5 μ M SRB (false red color). (B) Fluorescence intensity of NBD-PE measured inside the ROIs indicated in A (white circle – proportional to the GUV size) as a function of time. (C) High-resolution 3D image reconstructions of GUVs immobilized in 0.5% w/v agarose. Left: GUV composed of DOPG:SM:chol (3:5:2–molar ratio) with 0.1 mol% of DiI C18. Ld and Lo domains are visible as bright and dark regions in the GUV membrane, respectively. Cross-sections (262 in total) were acquired at 512×512 pixels and 400 Hz scanning speed. Right: GUV made of made SM (in the gel phase) with 0.1 mol% DiI C18. Cross-sections (100) were acquired at 512×512 pixels and 400 Hz scanning speed. (D) Confocal snapshots of a GUV labeled with 0.5 mol% NBD-PE (green) dispersed in 0.5% w/v agarose and encapsulating 2.5 μ M SRB (red). The images show the vesicle before and after membrane poration induced by an applied DC pulse (3 kV/cm, 150 μ s). The pore region corresponds to the membrane discontinuity segment. Numbers correspond to time relative to the application of the pulse. The electric field direction is shown as an arrow. All scale bars correspond to 10 μ m.

One question that arises when immobilizing the vesicles is whether the jellification process leads to shrinking or rupturing of the larger ones due to possible mechanical strain. We thus examined the effect of immobilization on GUV stability and on membrane permeability. The size distributions of GUV populations in the presence and absence of agarose are nearly the same (see Fig. S3), showing that even large vesicles remain stable in the presence of agarose, in contrast to results with other immobilization protocols¹⁸. This observation indicates that jellification proceeds only in the solution around the vesicles, surrounding them in cages. Note that the jellification process does not change significantly the solution osmolarity (the molar concentration of 1% w/v agarose is less than 1.5 mM²¹). We assume that agarose is depleted from a thin region around the vesicles, allowing them to perform shape fluctuations (see online movie). Importantly, populations of GUVs encapsulating the aqueous probe sulforhodamine B (SRB) were monitored for at least 1 h. Permeable GUVs were never observed for hundreds of vesicles analyzed.

Forcedly induced pores in immobilized vesicles fully reseal. GUVs have been used in a number of studies investigating pores in membranes, whether generated by pore-forming agents, see e.g.^{22–26}, or induced externally, e.g. by electric fields^{27,28}. We questioned the applicability of GUV immobilization for such studies. In particular, we investigated whether the resealing of large pores in the membrane would be prevented by the agarose gel as recently observed for GUVs containing agarose in their interior²⁹. To induce the micron-sized pores (macropores), we exposed immobilized GUVs to strong electric pulses. The macropores fully resealed and membrane integrity was completely restored (see Figs 1D and S4). Leakage of the internal content occurred only during the time when the macropore was open (see Fig. S5). This finding is important, because it demonstrates that while pores in vesicles grown on hybrid films of agarose and lipids (following the protocol in ref. 30) do not reseal, GUVs immobilized post formation can be employed for studies with pore-forming molecules provided they do not interact with agarose (a detailed description of how agarose in the internal and external media affects vesicle deformation, poration and relaxation dynamics is presented in section S4 of the Supplementary Information).

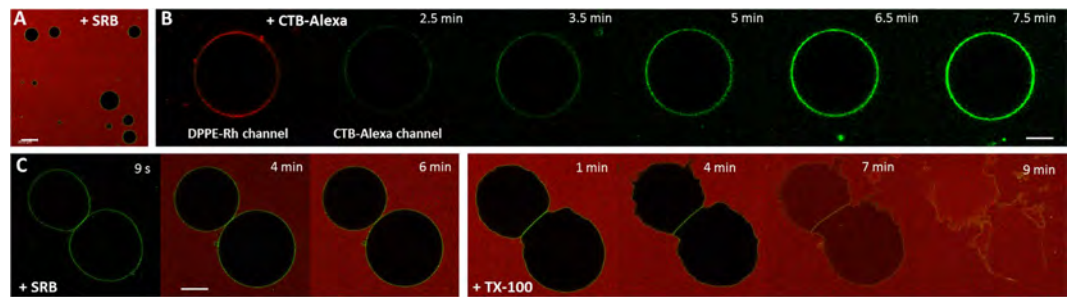


Figure 2. Diffusion of water-soluble molecules in the agarose gel. (A) Field with several immobilized GUVs (POPC with 0.5 mol% NBD-PE, green) obtained ~15 min after addition of an aliquot of SRB (red) to yield a final 2.5 μM concentration. Scale bar represents 50 μm . (B) Confocal microscopy images of an immobilized GUV (POPC with 1 mol% GM1 and 0.1 mol% DPPE-Rh, red channel) acquired after addition of CTB-Alexa (green channel) to yield a final 25 ng/mL concentration. The scale bar represents 10 μm . (C) Confocal microscopy images of two GUVs (POPC with 0.5 mol% NBD-PE, green). An aliquot of SRB (red) was added to the chamber with immobilized vesicles to yield a final 2.5 μM concentration. After establishing homogenous distribution of SRB in the chamber (6 min), an aliquot of TX-100 was added to the same sample to yield a final concentration of 1 mM (above its critical micelle concentration and therefore able to solubilize the membranes). The time stamp refers to the moment when SRB or TX-100 were added to the chamber with immobilized GUVs. The scale bar represents 20 μm .

Indeed, we expect that while the dynamics of resealing of pores in the micrometer range is slowed down, the closure of nanometer-sized pores would not be affected. The results broadly validate that the mechanical confinement provided by agarose does not affect the vesicle structural integrity and does not hinder the complete resealing of membrane pores even in conditions where they were forcedly induced.

Water-soluble molecules can freely diffuse through the agarose mesh. If the agarose gel does not hinder the diffusion of water-soluble molecules and particles, our protocol could then be applicable to study their binding to the membrane. Thus, we attempted to determine whether molecules and particles added to the chamber after agarose jellification can freely diffuse through the agarose mesh and reach the immobilized vesicle. To test that, different molecules were added to the observation chamber after immobilization of GUVs (see Fig. S1 for a sketch): the inert and small aqueous dye SRB (0.6 kDa), the detergent TX-100 (0.6 kDa monomers forming ~90 kDa micelles above 0.3 mM), which solubilizes the membrane, and cholera toxin B labeled with Alexa 488 (CTB-Alexa), a pentameric protein (~57 kDa) that binds to GM1 gangliosides present on the membrane surface. In a first experiment, SRB was added to the chamber with already immobilized vesicles (see Fig. S1). After about 10 min, the SRB fluorescence was homogeneous throughout the chamber and the GUVs remained impermeable to the dye (Fig. 2A). In a second experiment, CTB-Alexa was added to the chamber with immobilized GUVs made of POPC doped with 1 mol% GM1 and 0.1 mol% DPPE-Rh. The protein CTB-Alexa was able to freely diffuse through the agarose gel and within less than 10 min reach the vesicles and bind to their surface (Figs 2B and S6). In a third experiment, the ability of TX-100 micelles (~5 nm) to reach and solubilize immobilized POPC GUVs was tested. Initially, SRB was added and in less than 10 min its distribution in the chamber was homogeneous (Figs 2C and S6). Afterwards, an aliquot of the detergent TX-100 was added and the same vesicles were followed over time. After a few minutes, the detergent reached the selected vesicles and solubilized them (the last snapshot of Fig. 2C shows the solubilization process, which eventually finishes with no remaining bilayer structures—image not shown). Area expansion due to incorporation of TX-100 into the bilayer as reported earlier²⁵ could be observed here as well and was not significantly hindered by the agarose scaffold (see snapshots 1–4 min in Fig. 2C). The three types of experiments consistently demonstrate that water-soluble molecules and particles with sizes up to ~5 nm (corresponding to the size of the TX-100 micelles), with no specific affinity for agarose, can diffuse through the mesh and eventually reach the GUV surface even when externally added to the gel after immobilization of the GUVs. Thus, our protocol opens possibilities for applications where interactions of molecules and nanoparticles with the membrane (involving processes such as binding, pore formation and solubilization) can be directly studied on immobilized vesicles.

To explore more precisely the influence of the agarose gel on the diffusion of small molecules such as SRB, we used FCS to measure the diffusion coefficient (D) of SRB in the presence and absence of the agarose gel. For such molecules, FCS is preferred over FRAP since the former technique is more suitable to study fast moving objects. Fig. S7A shows a typical autocorrelation curve for SRB in solution with the corresponding fit and the diffusion coefficient values obtained in the presence and absence of 0.5% w/v agarose. The mean values obtained were $D = 404 \pm 25 \mu\text{m}^2/\text{s}$ (no agarose) and $D = 414 \pm 10 \mu\text{m}^2/\text{s}$ (in 0.5% w/v agarose), comparable to data in the literature^{31,32}. Diffusion coefficient assessed with FCS probes short-range displacements (within the confocal volume). To probe long-range diffusion, FRAP measurements were performed with the aqueous probe carboxyfluorescein (CF, 0.4 kDa) in the presence and absence of 0.5% w/v agarose using a large photobleaching spot (20 μm diameter). The diffusion coefficients obtained in both cases are equal within the experimental error: $D = 367 \pm 60$ and $417 \pm 75 \mu\text{m}^2/\text{s}$ for CF in water and in agarose gel, respectively, as shown in Fig. S7B. These results corroborate our finding that the diffusion of small molecules is not affected by the agarose mesh at the agarose concentration used here, at least up to the micrometer range. In fact, previous results showed unhindered diffusion of

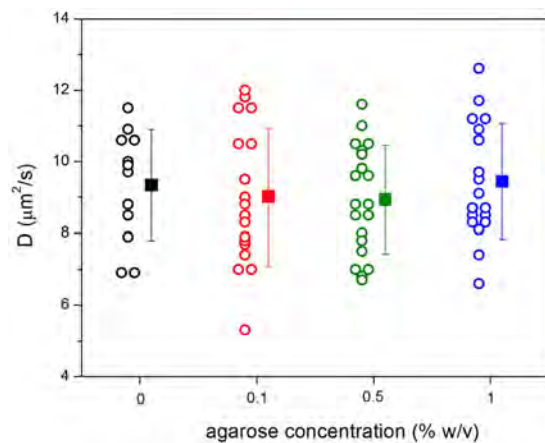


Figure 3. Lipid diffusion coefficient D as a function of agarose concentration in the vesicle exterior.

Each point represents a single FRAP measurement on an individual GUV and the mean values with standard deviation for every agarose concentration are indicated. The GUVs were composed of POPC with 1 mol% NBD-PE.

macromolecules (<10 nm) in the presence of even higher agarose concentrations (1.5% w/v agarose)³³. Therefore, the immobilization strategy shown here can be used to study the effect of various water-soluble (macro)molecules on membrane properties.

The presence of the agarose gel does not affect lipid diffusion. The diffusion coefficient of NBE-PE lipids in immobilized GUVs was measured with FRAP for increasing agarose concentrations and compared with data collected on agarose-free (non-immobilized) GUVs. Photobleaching was performed on the vesicle poles and diffusion during photobleaching was taken into account in the determination of the diffusion coefficient (see Experimental Section and ref. 34). FRAP measurements on non-immobilized vesicles is challenging and a large number of data ($>50\%$) had to be discarded due to significant GUV drift during measurements or artifacts in the recovery curves. In contrast, FRAP is very easy to perform on agarose-immobilized GUVs. Figure 3 shows values of the diffusion coefficients obtained on POPC GUVs at increasing agarose concentration. The mean values measured for each agarose concentration were $D = 9.3 \pm 1.6$ (0%), 9.0 ± 1.9 (0.1%), 8.9 ± 1.5 (0.5%) and 9.4 ± 1.6 (1%) $\mu\text{m}^2/\text{s}$. These values are in the upper range of values reported in the literature (3–10 $\mu\text{m}^2/\text{s}$) from different model systems using different techniques^{1,35–39}. However, most of the reported FRAP data^{35,38} were analyzed without correcting for diffusion during photobleaching, and are probably underestimated, as discussed in ref. 34. More importantly, the above results show that lipid diffusion in the GUVs is unhindered and agarose has no effect on lipid lateral mobility even at relatively high agarose concentrations.

Applying GUV immobilization to measure the mobility of lipids in different conditions. Above, we demonstrated that vesicle immobilization in agarose allows facile imaging and can be potentially used for precise quantification of membrane properties. The applications that we will now consider address the role of membrane phase state and charge on lipid mobility.

Lipid diffusion is strongly influenced by the phase state of the membrane. Of special biological relevance are liquid phases with properties modulated by the presence of cholesterol. As shown in Fig. 1C (left), ternary lipid mixtures can exhibit Lo/Ld phase coexistence, relevant for studies on raft-like systems. It is well known that lipid mobility is strongly reduced in the Lo phase compared to the Ld phase⁴⁰. GUV immobilization not only enables precise quantification of the lipid lateral mobility in each of the phases but allows such measurements to be performed on the same vesicle. Such experiments are challenging to conduct on freely suspended GUVs. Here, FRAP measurements were performed in the Lo and Ld phases of fully phase-separated GUVs made of DOPG:SM:chol 3:5:2 and immobilized in agarose. For such experiments, a photostable dye with preferential partitioning in one phase but present in both phases, is required. DiI C18 fulfills these requirements and is known to prefer the Ld phase⁴¹, which appears brighter. FRAP was performed in the vesicle equator (Fig. 4A) instead of at the pole regions, since each domain was not necessarily present at the vesicle poles. Recovery data for Ld and Lo phases performed in the same GUV (with domains equatorially opposite to each other to avoid polarization effects) are shown in Fig. 4B, with half-time ($t_{1/2}$) of full recovery being 1.5 and 17.7 s, respectively. Since the geometry of the bleached area in the equator is different from that on the vesicle poles, the analysis discussed in eqs. 1 and 2 to extract the diffusion coefficient from the recovery curves cannot be directly applied here. Therefore, Fig. 4C shows the ratio of $t_{1/2}$ obtained for the Lo and Ld phases in the same vesicle, which should be proportional to the ratio between the diffusion coefficients of the two phases, D_{Ld}/D_{Lo} . The scatter in the data probably reflects the scatter in membrane composition within the batch resulting from the preparation method⁴². The results show that, for this membrane composition, diffusion in the Ld phase is ~ 7 times faster than that in the Lo phase, similarly to data reported for neutral GUVs^{40,43}. Note that the value of the ratio will depend on the exact vesicle composition, where the domain compositions are defined by the tie line. To summarize, we demonstrate the utility of the

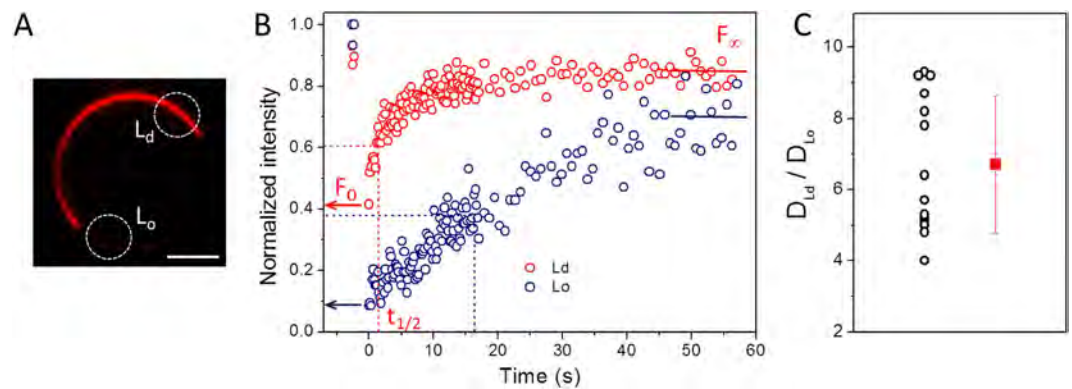


Figure 4. GUV immobilization allows quantification of lipid lateral mobility in phase separated membranes. (A) Confocal cross section of a DOPG:SM:chol (3:5:2-molar ratio) GUV immobilized in 0.5% w/v agarose. The membrane is labeled with 0.1 mol% of DiI C18. Ld and Lo domains are visible as bright and weakly fluorescent regions in the GUV membrane, respectively. Scale bar: 10 μm . (B) FRAP recovery data for Ld (red) and Lo (blue) domains performed on the ROIs (marked with dashed white circles in (A)). F_0 , $t_{1/2}$ and F_∞ are the initial fluorescence after photobleaching, the half-time of recovery and the fluorescence after recovery, respectively. (C) Ratio of half-time of recovery $t_{1/2}$ for the Lo and Ld domains obtained on the same vesicle. Each point represents a single GUV.

agarose-based immobilization method to perform FRAP measurements on different domains in the very same phase-separated GUV.

Next we examined the role of membrane charge on the lipid diffusion of homogeneous fluid membranes. The general understanding in the literature is that lipid mobility is reduced in charged membranes^{35,36,44}. The diffusion coefficient experiments here were performed on the poles of immobilized GUVs composed of pure POPC, POPC:POPG 1:1 (molar ratio) and pure POPG. The effect of membrane charge on the diffusion coefficient was probed using both FRAP and FCS and the results are summarized in Fig. 5. The measured diffusion coefficient decreases as the fraction of anionic lipids increases. This trend is observed both with FRAP and FCS measurements. FRAP yields slightly higher values presumably because of the different probe used and because of differences in the measurement techniques³⁸. The consistent trends indicate that reduction in lipid mobility is a true behavior rather than an experimental bias. In Table S1, we have compiled values of diffusion coefficients measured with both techniques.

Small liposomes can also be immobilized by the agarose gel. Small liposomes (~100 nm diameter) are extensively used as biomimetic membrane model in a wide variety of applications. Very often, in studies investigating binding of molecules to the membrane or bilayer-assisted reactions, liposome clustering or aggregation occurs, see e.g. refs 45,46. Approaches have been reported by which aggregation may be avoided, for example via coating of the liposomes with steric inhibitors, such as polyethylene glycol⁴⁷. This approach, however, might hinder the investigated interaction. Dispersion of liposomes in agarose gel could be used as another effective means to suppress aggregation by significantly reducing liposome mobility and hence the likelihood of contact between liposomes.

We used the agarose gel method to test whether small liposomes could also be efficiently immobilized. A suspension of fluorescently labeled liposomes (at total lipid concentration of 20 μM) was investigated at increasing concentrations of agarose. To quantify the mobility of the liposomes, their trajectories were recorded for 30 seconds using confocal microscopy. In the absence of agarose, the liposomes could not be individually tracked due to their fast movement. At 0.1% w/v agarose, individual liposomes could be followed and their movements spanned distances of several micrometers (black data in Fig. 6A). Liposome mobility was significantly reduced when the polymer concentration was increased to 0.25% w/v (blue data) and was virtually suppressed upon further increase to 0.5% w/v agarose (red data). Another approach to probe liposome mobility based on detection of moving particles inside a ROI is shown in Fig. S8. The liposomes were immobilized in most areas of the observation chamber at 0.5% w/v agarose concentration, but they were still able to display μm -length displacement in certain regions (mostly at the chamber edges), probably due to inhomogeneous mixing. Nonetheless, these results demonstrate that small liposomes can be completely immobilized inside the gel at similar agarose concentration as that used for GUV immobilization. This finding opens up new possibilities to perform quantitative measurements on small particles or liposomes as demonstrated below.

As an example, we investigated a protein-lipid reaction that is usually accompanied by vesicle aggregation. The autophagy-related protein Atg8 is known to covalently bind to phosphatidylethanolamine (PE) in eukaryotic membranes in a complex conjugation reaction involving two additional proteins, Atg3 and Atg7, and ATP⁴⁸. Membranes containing Atg8-PE were shown to aggregate *in vivo* and *in vitro*⁴⁸⁻⁵¹. Thus, hindering aggregation of liposomes with Atg8-PE is important for quantifying the protein coverage on membranes. Here, we investigated the influence of the agarose gel on the complex biochemical reaction of Atg8-PE conjugation and the ability of agarose to prevent liposome aggregation.

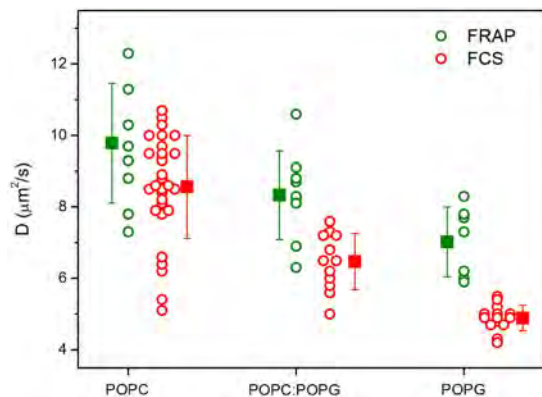


Figure 5. Diffusion coefficient D measured for 1 mol% NBD-PE (FRAP, green) or 0.002 mol% DiI C18 (FCS, red) in neutral (pure POPC) and charged (POPC:POPG 1:1 and pure POPG) GUVs immobilized in 0.5% w/v agarose. Each point represents a measurement on different GUV (for FRAP, one measurement per GUV was performed whereas for FCS, up to three measurements per vesicle were performed). The squares are mean values with standard deviations.

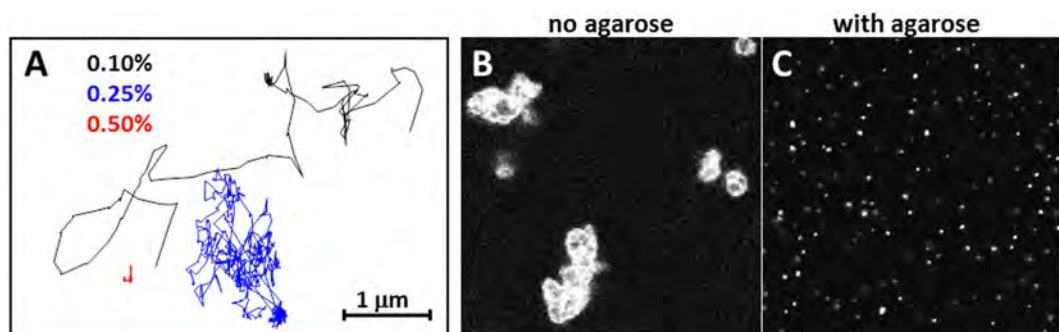


Figure 6. Immobilization of LUVs in agarose gels. (A) Trajectories of single fluorescently labeled 100-nm liposomes (DOPE:DOTAP:DPPE-Rh 1:1:0.1 mol) tracked during 30 s (150 ms/frame) in the presence of 0.1 (black), 0.25 (blue) and 0.5 (red) % w/v agarose. (B) Atg8-PE induced liposome (DOPE:POPC:chol:POPG 63.6:13.6:13.6:9.1) aggregates in the absence of agarose. (C) Liposome aggregation by Atg8-PE is prevented by addition of 0.5% w/v agarose. Individual protein-labeled liposomes are clearly observed. In panels B and C, the fluorescence signal is from fluorescently labeled Atg8. The picture dimensions are $110\ \mu\text{m} \times 110\ \mu\text{m}$.

Atg8 was fluorescently labeled^{48,49} and added, together with Atg3, Atg7 and ATP, to non-labeled freely-suspended and agarose-immobilized PE-containing liposomes. As expected, the Atg8-PE binding reaction induced strong liposome aggregation in agarose-free solution (Fig. 6B). In sharp contrast, carrying out the same reaction with immobilized liposomes does not lead to vesicle aggregation and single individual fluorescent spots corresponding to protein-bound liposomes are clearly seen as diffraction-limited spots (Fig. 6C). The results also show that the proteins are able to diffuse through the agarose meshwork as shown for other molecules in Fig. 2. Our results demonstrate that the complex biochemical reaction involving Atg8, Atg3, Atg7 and ATP occurred on the liposome surface even in the presence of the agarose mesh. Moreover, liposome immobilization effectively prevented vesicle aggregation. In conclusion, the agarose immobilization method can be applied to any liposomal system and enables users to perform quantitative single-liposome experiments in a simple way.

Concluding Remarks

In this work, we developed a simple method to efficiently immobilize lipid vesicles of various sizes, from 100 nm to $100\ \mu\text{m}$. The approach is based on confining the vesicles by agarose gel in the external medium. In the conditions studied here, giant vesicles are fully immobilized for times much longer (several minutes) than conventionally probed in experiments. Immobilization does not damage the vesicles and membrane integrity is restored even after the vesicles are exposed to drastic perturbation such as electroporation. Molecules, proteins and nanoparticles (with sizes below or equal to 5 nm) added after vesicle immobilization can freely diffuse through the mesh, reach the vesicles and interact with the membrane in the same way as in the absence of agarose. Importantly, the presence of the agarose gel has no detectable effect on the lateral diffusion of lipids. We applied the method to perform quantitative measurements, which are challenging and very difficult to establish without an immobilization strategy. As a proof of principle, we showed that the lipid diffusion coefficient is strongly dependent on membrane phase state and that it is reduced at increasing membrane charge density in fluid membranes.

As demonstrated in this work, the overall membrane structure and its permeability and fluidity are preserved after immobilization. However, a word of caution should be added: for some GUV-based experimental approaches, which probe the morphological responses of vesicles, such as electrodeformation^{29,52} and induction of membrane curvature⁵³, immobilization might lead to adverse effects which should be carefully considered before employing this approach. For example, even though immobilized GUVs with excess area display visible shape fluctuations (see supplementary movie), the influence of agarose on the membrane bending stiffness using fluctuation spectroscopy (see e.g. ref. 54) was not quantified here because of potential interference of the gel on the vesicle contour detection.

The detailed internal structure of the agarose polymer is not known, but it is expected to form compartments of different sizes depending on a number of factors such as temperature, T_m of the used agarose type, agarose concentration and cooling speed. FCS measurements of diffusion coefficient of small probes inside a 1.5% w/v low T_m agarose yields pore size of ~70 nm and show anomalous diffusion for particles above 10 nm in size³³. Estimates from absorbance measurements for low T_m agarose at 1% w/v and room temperature yield large pore sizes ~600 nm⁵⁵. Based on our data, small molecules such as CF (0.4 kDa) and SRB (0.6 kDa), the proteins CTB, Atg3, Atg7 and Atg8 (13.6–71 kDa) and TX-100 micelles (~90 kDa; ~5 nm) are able to diffuse through the mesh. On the other hand, 100 nm liposomes are virtually immobilized in the presence of 0.5% w/v agarose. Therefore, we can conclude that at 0.5% w/v agarose, the compartment size should be smaller than 100 nm. This mesh size enables complete immobilization of micro and large structures such as liposomes and GUVs whereas the diffusional mobility of small molecules, proteins and micelles is preserved. This opens the possibility to study the interaction of various macromolecules and nanoparticles with the membrane of immobilized GUVs. We also expect that the immobilization strategy will allow performing permeabilization studies such as in refs 56,57.

We envision the agarose immobilization method to find a broad application as it allows long term imaging of vesicles without compromising the membrane structural integrity. Apart from the applications reported here, state-of-the-art super-resolution microscopy techniques, such as STED, STED-FCS and PALM/STORM microscopy^{58,59}, will also profit from the agarose immobilization method, since one requires a reliable way of immobilization to achieve the stated resolution precision in the 20–30 nm range. In summary, the agarose immobilization method described here allows detailed quantitative investigation of biophysical membrane properties of giant and small vesicles with unprecedented simplicity.

Experimental Section

Materials. The lipids 1-palmitoyl-2-oleoyl-sn-glycero-3-phosphocholine (POPC), 1-palmitoyl-2-oleoyl-sn-glycero-3-phospho-(1'-rac-glycerol), sodium salt (POPG), 1,2-dioleoyl-sn-glycero-3-phosphoethanolamine (DOPE), 1,2-dioleoyl-3-trimethylammonium-propane, chloride salt (DOTAP), egg (chicken) sphingomyelin (SM), Ganglioside (Ovine Brain) (GM1) and cholesterol and the fluorescent probes 1-palmitoyl-2-6-[(7-nitro-2-1,3-benzoxadiazol-4-yl)amino]hexanoyl]-sn-glycero-3-phosphoethanolamine (NBD-PE) and 1,2-dipalmitoyl-sn-glycero-3-phosphoethanolamine-N-(lissamine rhodamine B sulfonyl) (DPPE-Rh) were purchased from Avanti Polar Lipids (Alabaster, AL). The fluorescent probe 1,1'-Diocadecyl-3,3,3',3'-Tetramethylindocarbocyanine Perchlorate (DiI C18) was obtained from Life Technologies (Carlsbad, CA). Low-melting temperature agarose was obtained from Fischer Scientifics (Waltham, MA) and Cholera Toxin Subunit B (Recombinant) Alexa Fluor 488 Conjugate (CTB-Alexa) was purchased from Invitrogen (Carlsbad, CA). The fluorescent dye sulforhodamine B (SRB), carboxyfluorescein (CF), the detergent Triton X-100 (TX-100) and all other chemicals were purchased from Sigma Aldrich (St. Louis, MO). All chemicals were used without further purification. Milli-Q water was used throughout the work.

Preparation of giant and large unilamellar vesicles. GUVs were produced by the electroformation method⁶⁰ with minor modifications. In brief, 5–8 μ L of a given 3 mM lipid stock solution in chloroform were homogeneously spread on a pair of conductive ITO glasses and dried for 5 minutes under N_2 stream. A 2 mm-thick Teflon spacer was used to create a chamber between the glasses, which was then sealed and filled with a 0.2 M sucrose solution. The chamber was connected to a function generator and an AC field (1.2 V, 10 Hz) was applied at room temperature for 1 h to swell the GUVs. Only when containing agarose inside, vesicles were grown at 70 °C. When fluorescent lipids were included, GUV growth was performed in the dark. Afterwards, the GUVs were diluted ~7 fold in isoosmolar glucose solution containing or not fluid agarose. For the phase-separated membrane composition and pure SM, lipid hydration was performed at 60 °C and with 50 mM sucrose, 2 mM HEPES and 1 mM EDTA, and the vesicles were then dispersed in hypotonic 40 mM glucose solution.

Liposomes were prepared by extrusion at room temperature. A chloroform solution of DOTAP:DOPE:DPPE-Rh (1:1:0.1 molar ratio) was placed in a round-bottom test tube. The chloroform was evaporated with a N_2 stream and the test tubes were further dried under vacuum for 2 h. The lipid film was then hydrated with a 0.2 M sucrose solution to yield a final 2 mM lipid concentration and vigorously vortexed for 2–5 minutes. The multilamellar vesicles obtained were subjected to 11 cycles of extrusion through a 100 nm pore diameter polycarbonate membrane (Whatman, Maidstone, UK). To test liposome mobility as a function of agarose concentration, the liposome dispersion was diluted to 20 μ M. In all cases, experiments were performed at room temperature. The liposomes conjugated to autophagy-related proteins were prepared by freeze-thaw cycling (see next section for details).

Interaction of Atg8 with liposomes. The autophagy-related proteins Atg8, Atg7 and Atg3 were purified and Atg8 was labeled with Alexa 488 as reported previously^{48,49}. Liposomes composed of 63.6 mol% DOPE, 13.6 mol% POPC, 13.6 mol% cholesterol and 9.1 mol% POPG were suspended in 50 mM Tris-HCl pH 8, 10 mM NaCl, 0.1 mM $MgCl_2$. The agarose was dissolved in the same buffer at a final concentration of 1% w/v. The proteins were mixed with the liposomes in the presence of ATP (1.2 μ M Atg8, 0.2 μ M Atg7, 0.2 μ M Atg3, 0.7 mM

lipid, 2 mM ATP) and then diluted 1:1 with 1% w/v agarose buffer in the fluid state. The samples were placed between cover slips sealed by silicon spacers and incubated for 1 min on ice to induce gelation of the agarose. For the Atg8 conjugation reaction, the samples were protected from light during incubation for 100 min at 22 °C and then analyzed by confocal microscopy.

Application of DC pulses to GUVs. To examine vesicle deformability and monitor the effect of agarose on closure of pores in the membrane, GUVs containing agarose either internally or externally were exposed to an electric pulse applied in an electrofusion chamber (Eppendorf, Germany) with parallel cylindrical electrodes (92 μm radius) spaced at 500 μm. A single DC pulse of 150 V field strength and 150 μs duration was applied for all cases. Vesicle imaging was carried out using a Zeiss Axio Observer.D1 microscope equipped with a sCMOS camera (pco.edge, PCO AG, Kelheim, Germany). The vesicles were observed either with a 20x (NA 0.5) or a 40x (NA 0.6) objective in the phase contrast or epifluorescence mode. For fluorescence microscopy images, excitation (540–553 nm) and emission (575–640 nm) filters were used.

Confocal Microscopy. Confocal microscopy imaging, FRAP and FCS were performed on a Leica TCS SP5 (Wetzlar, Germany) with a 40x (0.75 NA) or 63x (1.2 NA) water immersion objectives and 1 Airy unit. NBD-PE, CTB-Alexa, CF and Alexa488-labeled Atg8 were excited with an argon laser at 488 nm and SRB, DiI C18 and DPPE-Rh with a diode-pumped solid-state laser at 561 nm. The emission signals were collected in the 490–545 nm and 575–630 nm bands, respectively. Image quantification was performed with the Leica software (Leica application Suite) or ImageJ. For liposome tracking, a spot tracker plug-in from ImageJ was used as in ref. 61.

Fluorescence recovery after photobleaching (FRAP). For FRAP measurements on membranes, the GUVs contained the fluorescent probes NBD-PE (1 mol%) or DiI C18 (0.1 mol%). Images (296 × 296 pixels) were recorded in the bidirectional scan mode at 1000 Hz and pinhole at 1 Airy unit. Three images at attenuated laser intensity (below 5%) were taken before photobleaching. Photobleaching was performed using the argon 488 nm (for NBD) or the 561 nm laser (for DiI C18) at maximum intensity for 720 ms (4 frames) through a circular ROI of nominal radius $r_n = 2.5$ or $5 \mu\text{m}$. The laser was then switched back to attenuated intensity and the recovery images were recorded for several seconds. If not explicitly mentioned, photobleaching was performed on the upper or lower GUV surface. For FRAP of the aqueous probe CF, a concentrated CF solution was first prepared in ethanol (200 mM) and then diluted in water or in 0.5% w/v agarose to give a final working concentration of $0.2 \mu\text{M}$ CF. Images (296 × 296 pixels) were recorded in the bidirectional scan mode at 1400 Hz and pinhole at 1 Airy unit. Ten pre-bleach images (98 ms/frame) at attenuated intensity (10% with the 488 nm laser line) were taken before and five bleaching iterations (0.49 s) using the 458, 476, 488 and 496 laser lines at maximum intensity to bleach CF, with a nominal radius $r_n = 10 \mu\text{m}$. After bleaching, excitation at 488 nm was switched back to attenuated intensity.

Several ways to extract the diffusion coefficient D from FRAP recovery curves have been reported in the literature^{62–64}. Here, the data were analyzed according to a simplified equation considering molecular diffusion during photobleaching³⁴, hence reducing error. The diffusion coefficient D is given as:

$$D = \frac{r_e^2 + r_n^2}{8t_{1/2}} \quad (1)$$

where r_e and r_n are the effective and the nominal (i.e., user-defined) bleaching radii and $t_{1/2}$ is the half-time of fluorescence recovery (i.e., the time to reach $F_{1/2} = (F_0 + F_\infty)/2$, where F_0 and F_∞ are the fluorescence intensity in the first post-bleach image and after full recovery, respectively; see Fig. S9). To obtain the effective bleaching radius r_e , the fluorescence intensity line profile $f(x)$ through the center of the bleaching spot in the first post-bleaching image was fitted with the expression

$$f(x) = 1 - K \exp\left(-\frac{2x^2}{r_e^2}\right) \quad (2)$$

where K is the bleaching depth. Determination of r_e in our setup is shown in the Supplementary Information (Fig. S9) and the values used were $r_e = 7$ (for $r_n = 2.5 \mu\text{m}$) and 9 (for $r_n = 5 \mu\text{m}$) μm. A typical recovery curve is also shown (Fig. S9).

Fluorescence correlation spectroscopy (FCS). FCS measurements were performed with water-soluble (SRB) and membrane-embedded (DiI C18) fluorescence probes with a 63x (1.2 NA) water immersion objective. The sample was excited at 561 nm and fluorescence emission was collected in the band 607–683 nm using a filter cube. Photon counting was accomplished by avalanche photodiodes (Leica, Wetzlar, Germany) and time correlations were calculated at a sampling frequency of 200 kHz. Initially, to determine the geometry of the FCS volume, the correlation curves obtained from 10 nM SRB in 0.2 M sucrose were fitted globally with a 1-component 3D diffusion model with a fixed diffusion time of $D = 410 \mu\text{m}^2/\text{s}$ ^{31,32}:

$$G(\tau) = \frac{2\sqrt{2}}{\pi\sqrt{\pi} w_0^2 z_0 C} \frac{1}{\left(1 + \frac{8D\tau}{w_0^2}\right) \sqrt{1 + \frac{8D\tau}{z_0^2}}} \quad (3)$$

where C is the average molecule concentration in the FCS volume and τ the average time of the molecule in the focus volume. From the fit, the lateral and axial lengths of the FCS volume were obtained: $w_0 \approx 0.29 \mu\text{m}$ and

$z_0 \approx 2.31 \mu\text{m}$, respectively. Then, measurements of 10 nM SRB inside and outside immobilized GUVs were performed and eq. 3 was used to extract the diffusion coefficient D in the presence and absence of the agarose gel, respectively. The dye was present in the (fluid) glucose solution with agarose in which the GUVs were dispersed. At least 3 measurements were obtained per data point.

For FCS performed on GUV membranes, DiI C18 (0.002 mol%) was also excited using the 561 line. The obtained correlation curves were fitted using a 1-component 2D diffusion model:

$$G(\tau) = \frac{1}{\pi w_o^2 C} \frac{1}{\left(1 + \frac{4D\tau}{w_o^2}\right)} \quad (4)$$

The confocal volume was positioned either at the top or at the bottom of the vesicles to yield the maximum photon count. To minimize artifacts, the average number of fluorescent molecules was plotted as a histogram and only the measurements that showed roughly the same apparent dye concentration (Fig. S10) were considered. This procedure does not alter the general trends but only reduces the measurement error. After correction, at least eight vesicles per population were considered.

References

- Bacia, K., Scherfeld, D., Kahya, N. & Schwille, P. Fluorescence correlation spectroscopy relates rafts in model and native membranes. *Biophys. J.* **87**, 1034–1043 (2004).
- Kenworthy, A. K. *et al.* Dynamics of putative raft-associated proteins at the cell surface. *J. Cell Biol.* **165**, 735–746 (2004).
- Eggeling, C. *et al.* Direct observation of the nanoscale dynamics of membrane lipids in a living cell. *Nature* **457**, 1159–U1121 (2009).
- Dao, M., Lim, C. T. & Suresh, S. Mechanics of the human red blood cell deformed by optical tweezers. *J. Mech. Phys. Solids* **51**, 2259–2280 (2003).
- Yoon, T. Y., Okumus, B., Zhang, F., Shin, Y. K. & Ha, T. Multiple intermediates in SNARE-induced membrane fusion. *Proc. Natl. Acad. Sci. USA* **103**, 19731–19736 (2006).
- Christensen, S. M. & Stamou, D. Surface-based lipid vesicle reactor systems: fabrication and applications. *Soft Matter* **3**, 828–836 (2007).
- Hatzakis, N. S. *et al.* How curved membranes recruit amphipathic helices and protein anchoring motifs. *Nat. Chem. Biol.* **5**, 835–841 (2009).
- Dimova, R. *et al.* A practical guide to giant vesicles. Probing the membrane nanoregime via optical microscopy. *J. Phys.: Condens. Matter* **18**, S1151–S1176 (2006).
- Walde, P., Cosentino, K., Engel, H. & Stano, P. Giant Vesicles: Preparations and Applications. *ChemBioChem* **11**, 848–865 (2010).
- Dimova, R. In *Advances in Planar Lipid Bilayers and Liposomes*. Vol. 16 (ed Aleš, Igljič) 1–50 (Academic Press, 2012).
- Kuhn, P. *et al.* A facile protocol for the immobilisation of vesicles, virus particles, bacteria, and yeast cells. *Integr Biol-Uk* **4**, 1550–1555 (2012).
- Sarmiento, M. J., Prieto, M. & Fernandes, F. Reorganization of lipid domain distribution in giant unilamellar vesicles upon immobilization with different membrane tethers. *Biochim. Biophys. Acta-Biomembr.* **1818**, 2605–2615 (2012).
- Lipowsky, R., Rouhiparkouhi, T., Discher, D. E. & Weikl, T. R. Domain formation in cholesterol-phospholipid membranes exposed to adhesive surfaces or environments. *Soft Matter* **9**, 8438–8453 (2013).
- Korlach, J., Reichle, C., Muller, T., Schnelle, T. & Webb, W. W. Trapping, deformation, and rotation of giant unilamellar vesicles in octode dielectrophoretic field cages. *Biophys. J.* **89**, 554–562 (2005).
- Delabre, U. *et al.* Deformation of phospholipid vesicles in an optical stretcher. *Soft Matter* **11**, 6075–6088 (2015).
- Robinson, T., Kuhn, P., Eyer, K. & Dittrich, P. S. Microfluidic trapping of giant unilamellar vesicles to study transport through a membrane pore. *Biomicrofluidics* **7**, 044105 (2013).
- Fidorra, M., Garcia, A., Ipsen, J. H., Hartel, S. & Bagatolli, L. A. Lipid domains in giant unilamellar vesicles and their correspondence with equilibrium thermodynamic phases: A quantitative fluorescence microscopy imaging approach. *Biochim. Biophys. Acta-Biomembr.* **1788**, 2142–2149 (2009).
- Esquembre, R., Pinto, S. N., Poveda, J. A., Prieto, M. & Mateo, C. R. Immobilization and characterization of giant unilamellar vesicles (GUVs) within porous silica glasses. *Soft Matter* **8**, 408–417 (2012).
- Kusters, I. *et al.* Taming Membranes: Functional Immobilization of Biological Membranes in Hydrogels. *Plos One* **6**, e20435 (2011).
- Tsumoto, K., Oohashi, M. & Tomita, M. Monitoring of membrane collapse and enzymatic reaction with single giant liposomes embedded in agarose gel. *Colloid. Polym. Sci.* **289**, 1337–1346 (2011).
- Normand, V., Lootens, D. L., Amici, E., Plucknett, K. P. & Aymard, P. New insight into agarose gel mechanical properties. *Biomacromolecules* **1**, 730–738 (2000).
- Tamba, Y. & Yamazaki, M. Single giant unilamellar vesicle method reveals effect of antimicrobial peptide magainin 2 on membrane permeability. *Biochemistry* **44**, 15823–15833 (2005).
- Ambroggio, E. E., Separovic, F., Bowie, J. H., Fidelio, G. D. & Bagatolli, L. A. Direct visualization of membrane leakage induced by the antibiotic peptides: Maculatin, citropin, and aurein. *Biophys. J.* **89**, 1874–1881 (2005).
- Tamba, Y. *et al.* Single GUV method reveals interaction of tea catechin (-)-epigallocatechin gallate with lipid membranes. *Biophys. J.* **92**, 3178–3194 (2007).
- Mattei, B., Franca, A. D. C. & Riske, K. A. Solubilization of Binary Lipid Mixtures by the Detergent Triton X-100: The Role of Cholesterol. *Langmuir* **31**, 378–386 (2015).
- Riske, K. A. In *Advances in Planar Lipid Bilayers and Liposomes*. Vol. 21 (eds Chandrashekar, V. Kulkarni, Aleš, Igljič & Rappolt, Michael) 99–129 (Academic Press, 2015).
- Dimova, R. *et al.* Giant vesicles in electric fields. *Soft Matter* **3**, 817–827 (2007).
- Dimova, R. *et al.* Vesicles in electric fields: Some novel aspects of membrane behavior. *Soft Matter* **5**, 3201–3212 (2009).
- Lira, R. B., Dimova, R. & Riske, K. A. Giant Unilamellar Vesicles Formed by Hybrid Films of Agarose and Lipids Display Altered Mechanical Properties. *Biophys. J.* **107**, 1609–1619 (2014).
- Horger, K. S., Estes, D. J., Capone, R. & Mayer, M. Films of Agarose Enable Rapid Formation of Giant Liposomes in Solutions of Physiologic Ionic Strength. *J. Am. Chem. Soc.* **131**, 1810–1819 (2009).
- Petrasek, Z. & Schwille, P. Precise measurement of diffusion coefficients using scanning fluorescence correlation spectroscopy. *Biophys. J.* **94**, 1437–1448 (2008).
- Culbertson, C. T., Jacobson, S. C. & Ramsey, J. M. Diffusion coefficient measurements in microfluidic devices. *Talanta* **56**, 365–373 (2002).
- Fatin-Rouge, N., Starchev, K. & Buffle, J. Size effects on diffusion processes within agarose gels. *Biophys. J.* **86**, 2710–2719 (2004).
- Kang, M., Day, C. A., Kenworthy, A. K. & DiBenedetto, E. Simplified Equation to Extract Diffusion Coefficients from Confocal FRAP Data. *Traffic* **13**, 1589–1600 (2012).

35. Frey, S. & Tamm, L. K. Membrane Insertion and Lateral Diffusion of Fluorescence-Labeled Cytochrome-C-Oxidase Subunit-Iv Signal Peptide in Charged and Uncharged Phospholipid-Bilayers. *Biochem. J.* **272**, 713–719 (1990).
36. Wagner, M. L. & Tamm, L. K. Reconstituted syntaxin1A/SNAP25 interacts with negatively charged lipids as measured by lateral diffusion in planar supported bilayers. *Biophys. J.* **81**, 266–275 (2001).
37. Kahya, N., Scherfeld, D., Bacia, K., Poolman, B. & Schwille, P. Probing lipid mobility of raft-exhibiting model membranes by fluorescence correlation spectroscopy. *J. Biol. Chem.* **278**, 28109–28115 (2003).
38. Guo, L. *et al.* Molecular diffusion measurement in lipid bilayers over wide concentration ranges: A comparative study. *Chemphyschem* **9**, 721–728 (2008).
39. Machan, R. & Hof, M. Lipid diffusion in planar membranes investigated by fluorescence correlation spectroscopy. *Biochim. Biophys. Acta-Biomembr.* **1798**, 1377–1391 (2010).
40. Koralchak, J., Schwille, P., Webb, W. W. & Feigenson, G. W. Characterization of lipid bilayer phases by confocal microscopy and fluorescence correlation spectroscopy. *Proc. Natl. Acad. Sci. USA* **96**, 8461–8466 (1999).
41. Casadei, B. R., Domingues, C. C., de Paula, E. & Riske, K. A. Direct Visualization of the Action of Triton X-100 on Giant Vesicles of Erythrocyte Membrane Lipids. *Biophys. J.* **106**, 2417–2425 (2014).
42. Bezlyepkina, N., Gracià, R. S., Shchelokovskyy, P., Lipowsky, R. & Dimova, R. Phase Diagram and Tie-Line Determination for the Ternary Mixture DOPC/eSM/Cholesterol. *Biophys. J.* **104**, 1456–1464 (2013).
43. Bacia, K., Schwille, P. & Kurzchalia, T. Sterol structure determines the separation of phases and the curvature of the liquid-ordered phase in model membranes. *Proc. Natl. Acad. Sci. USA* **102**, 3272–3277 (2005).
44. Gilmanshin, R., Creutz, C. E. & Tamm, L. K. Annexin-Iv Reduces the Rate of Lateral Lipid Diffusion and Changes the Fluid-Phase Structure of the Lipid Bilayer When It Binds to Negatively Charged Membranes in the Presence of Calcium. *Biochemistry* **33**, 8225–8232 (1994).
45. Domingues, T. M. *et al.* Interaction of the Antimicrobial Peptide Gomesin with Model Membranes: A Calorimetric Study. *Langmuir* **29**, 8609–8618 (2013).
46. Quemeneur, F., Rinaudo, M., Maret, G. & Pepin-Donat, B. Decoration of lipid vesicles by polyelectrolytes: mechanism and structure. *Soft Matter* **6**, 4471–4481 (2010).
47. Shibata, H., Yomota, C., Kawanishi, T. & Okuda, H. Polyethylene Glycol Prevents *in Vitro* Aggregation of Slightly Negatively-Charged Liposomes Induced by Heparin in the Presence of Bivalent Ions. *Biol. Pharm. Bull.* **35**, 2081–2087 (2012).
48. Knorr, R. L. *et al.* Membrane Morphology Is Actively Transformed by Covalent Binding of the Protein Atg8 to PE-Lipids. *Plos One* **9**, e115357 (2014).
49. Nakatogawa, H., Ichimura, Y. & Ohsumi, Y. Atg8, a Ubiquitin-like Protein Required for Autophagosome Formation, Mediates Membrane Tethering and Hemifusion. *Cell* **130**, 165–178 (2007).
50. Galush, W. J., Nye, J. A. & Groves, J. T. Quantitative fluorescence microscopy using supported lipid bilayer standards. *Biophys. J.* **95**, 2512–2519 (2008).
51. Sorre, B. *et al.* Nature of curvature coupling of amphiphysin with membranes depends on its bound density. *Proc. Natl. Acad. Sci. USA* **109**, 173–178 (2012).
52. Riske, K. A. & Dimova, R. Electro-deformation and poration of giant vesicles viewed with high temporal resolution. *Biophys. J.* **88**, 1143–1155 (2005).
53. Baumgart, T., Hess, S. T. & Webb, W. W. Imaging coexisting fluid domains in biomembrane models coupling curvature and line tension. *Nature* **425**, 821–824 (2003).
54. Gracià, R. S., Bezlyepkina, N., Knorr, R. L., Lipowsky, R. & Dimova, R. Effect of cholesterol on the rigidity of saturated and unsaturated membranes: fluctuation and electrodeformation analysis of giant vesicles. *Soft Matter* **6**, 1472–1482 (2010).
55. Narayanan, J., Xiong, J. Y. & Liu, X. Y. Determination of agarose gel pore size: Absorbance measurements vis a vis other techniques. *J Phys Conf Ser* **28**, 83–86 (2006).
56. Leite, Natália B. *et al.* PE and PS Lipids Synergistically Enhance Membrane Poration by a Peptide with Anticancer Properties. *Biophys. J.* **109**, 936–947 (2015).
57. Fuentes, G. *et al.* Pores Formed by Bax α 5 Relax to a Smaller Size and Keep at Equilibrium. *Biophys. J.* **99**, 2917–2925 (2010).
58. Hell, S. W. Far-Field Optical Nanoscopy. *Science* **316**, 1153–1158 (2007).
59. Hell, S. W. *et al.* The 2015 super-resolution microscopy roadmap. *J. Phys. D: Appl. Phys.* **48**, 443001 (2015).
60. Angelova, M. I. & Dimitrov, D. S. Liposome Electroformation. *Faraday Discuss.* **81**, 303–311 (1986).
61. Sage, D., Neumann, F. R., Hediger, F., Gasser, S. M. & Unser, M. Automatic tracking of individual fluorescence particles: Application to the study of chromosome dynamics. *Ieee T Image Process* **14**, 1372–1383 (2005).
62. Axelrod, D., Koppel, D. E., Schlessinger, J., Elson, E. & Webb, W. W. Mobility Measurement by Analysis of Fluorescence Photobleaching Recovery Kinetics. *Biophys. J.* **16**, 1055–1069 (1976).
63. Soumpasis, D. M. Theoretical-Analysis of Fluorescence Photobleaching Recovery Experiments. *Biophys. J.* **41**, 95–97 (1983).
64. Lopez, A., Dupou, L., Altibelli, A., Trotard, J. & Tocanne, J. F. Fluorescence Recovery after Photobleaching (Frap) Experiments under Conditions of Uniform Disk Illumination—Critical Comparison of Analytical Solutions, and a New Mathematical Method for Calculation of Diffusion Coefficient-D. *Biophys. J.* **53**, 963–970 (1988).

Acknowledgements

The financial support of FAPESP (11/22171-6 and 13/07246-5), INCT-FCx, Deutsche Forschungsgemeinschaft (DFG) via the IRTG 1524 and the Japan Society for the Promotion of Science (JSPS) are gratefully acknowledged. This work is part of the MaxSynBio consortium, which is jointly funded by the Federal Ministry of Education and Research of Germany and the Max Planck Society. We thank Minchul Kang for helpful discussions on FRAP analysis.

Author Contributions

K.A.R., R.B.L. and R.D. designed the study and the method. R.B.L. performed most of the experiments and analyses. J.S. did the FCS measurements and R.L.K. the liposome experiments with Atg8. R.B.L., R.D. and K.A.R. wrote the paper. K.A.R. and R.D. provided the reagents and supervised the project.

Additional Information

Supplementary information accompanies this paper at <http://www.nature.com/srep>

Competing financial interests: The authors declare no competing financial interests.

How to cite this article: Lira, R. B. *et al.* Posing for a picture: vesicle immobilization in agarose gel. *Sci. Rep.* **6**, 25254; doi: 10.1038/srep25254 (2016).



This work is licensed under a Creative Commons Attribution 4.0 International License. The images or other third party material in this article are included in the article's Creative Commons license, unless indicated otherwise in the credit line; if the material is not included under the Creative Commons license, users will need to obtain permission from the license holder to reproduce the material. To view a copy of this license, visit <http://creativecommons.org/licenses/by/4.0/>

Supplementary information

Posing for a picture: vesicle immobilization in agarose gel

Rafael B. Lira, Jan Steinkühler, Roland L. Knorr, Rumiana Dimova, Karin A. Riske

Online movie. Movie of a fluctuating POPC GUV (labeled with 0.1 mol% DiI C18) obtained with confocal microscopy. The GUVs were dispersed in 0.2 M glucose with 0.5% w/v agarose. After jellification of agarose, the chamber was opened and the gel was exposed to a hyperosmotic solution (0.3 M glucose) inducing deflation of the immobilized vesicles. Thermal shape fluctuations are clearly detected in the GUV and are not suppressed by the agarose mesh. Additionally, no attachments to the agarose cage are observed. The time is indicated in the movie. The vesicle size is approximately 8 μm .

S1. Observation chamber with agarose-immobilized GUVs.

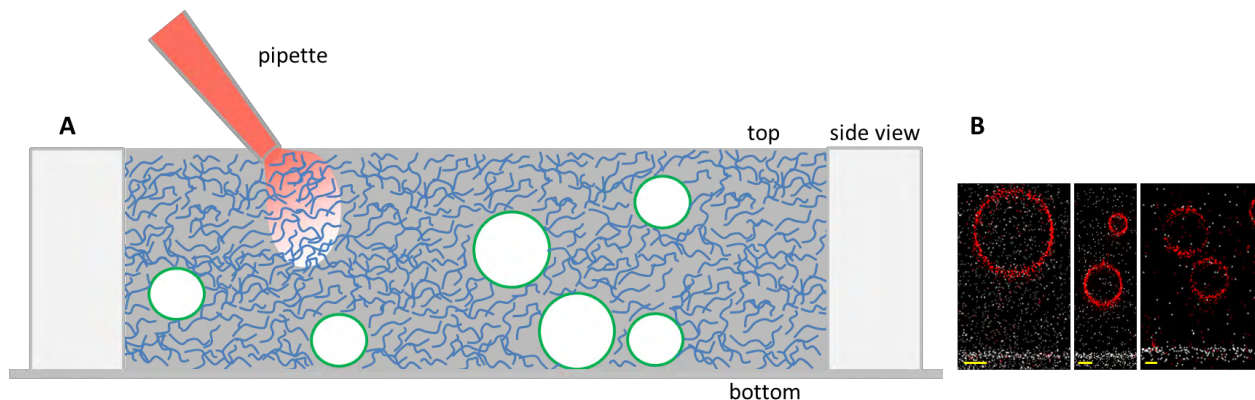


Figure S1. A) Sketch of the side view of the observation chamber. The GUVs are represented as green circles and agarose is shown in blue. GUVs were added with fluid agarose at high temperature (35-40 °C). After ~ 10 min and cooling to room temperature the agarose becomes a gel and GUVs get immobilized. Larger GUVs typically reached the chamber bottom before immobilization, but many GUVs were trapped in the agarose mesh before having sedimented to the chamber bottom. The chamber is closed by a glass slide from above. When the effect of molecules added post gelation is investigated, the glass slide is removed and the solution pipetted directly on the gel. After adding an aliquot of the investigated molecule (e.g. SRB, CTB-Alexa, TX-100), the chamber is reclosed with a cover slip and observation started. Alternatively, the molecule is added together with fluid agarose and the GUVs. B) Confocal microscopy images showing different cross sections (xz plane) of a chamber with POPC GUVs (labeled with 0.1 mol% DPPE-Rh) immobilized before reaching the bottom (white region below, observed under transmitted light). The scale bars represent 10 μm .

S2. Tubulation and deformation of a GUV in the presence of 1% w/v agarose.

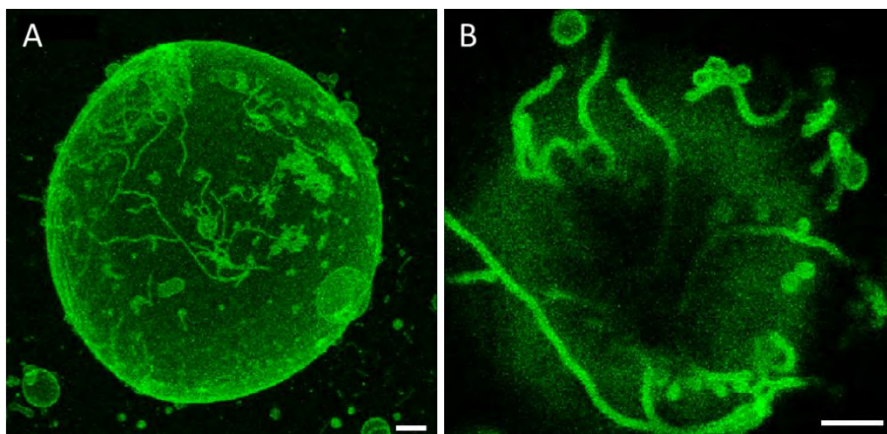


Figure S2. A) Three-dimensional reconstruction of a POPC GUV immobilized in 1% (w/v) agarose. Note that the vesicle is non-spherical and slightly deformed by the agarose gel. B) Image of the upper surface of the GUV shown in A. The formed tubes are always directed to the outside. Scale bars: 5 μm .

S3. Size distribution of GUVs in the presence and absence of agarose.

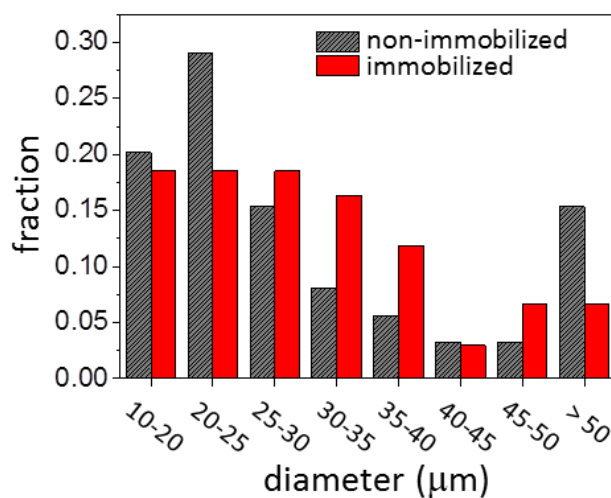


Figure S3. Vesicle size distributions from two typical batches of POPC GUVs in the presence (red, $n = 118$) and absence (black, $n = 111$) of agarose.

S4. Mechanical effects of agarose on GUVs

Recently, we showed that residual agarose present inside GUVs grown on hybrid films of agarose and lipids (following the protocol in Ref. ¹) significantly affects vesicle relaxation dynamics and membrane pore lifetime ². In the experiments shown here, where agarose was present exclusively outside, no adverse effects on vesicle size and stability were observed (Figure S3). In order to compare GUV mechanics in both conditions of agarose present exclusively in the vesicle exterior or interior, we followed the GUV response to electric fields. We applied a single and strong DC electric pulse to induce vesicle deformation and poration. In agarose-free aqueous solution, strong DC pulses deform and porate GUVs, after which the vesicle initial shape is restored with a characteristic relaxation time τ_{relax} and the formed macropores close with pore lifetime t_{pore} ³. Deformation is expressed as the aspect ratio of the vesicle semi-axes, a/b (see the inset in Figure S4). A typical GUV deformation/poration relaxation dynamic in agarose-free solution upon pulse application is shown in Figure S6 (black circles). Vesicle relaxation time for this particular GUV is $\tau_{\text{relax}} \sim 20$ ms. The horizontal line denotes the time period in which pores are optically detected, i.e. t_{pore} ; in this case $t_{\text{pore}} \sim 40$ ms. Both values are in agreement with previous data ^{2,3}. After pore closure, the vesicle integrity is restored. For experiments with agarose inside, GUVs were grown with a sucrose solution containing 0.5 % w/v fluid agarose (at a temperature above agarose T_m) and then dispersed in glucose solution. At room temperature, all vesicles in the batch displayed an internal gel-like polymer mesh (see Figure S5A) and membrane fluctuations were largely suppressed. When a strong pulse is applied to GUVs encapsulating agarose, vesicle deformation is inhibited ($a/b \sim 1$, red triangles in Figure S4), very large pores open and the polymer mesh is expelled (Figures S5A and S5B). The formed pore never reseals due to the physical obstruction induced by the mesh (Figures S5A and S5B), a process reported earlier ².

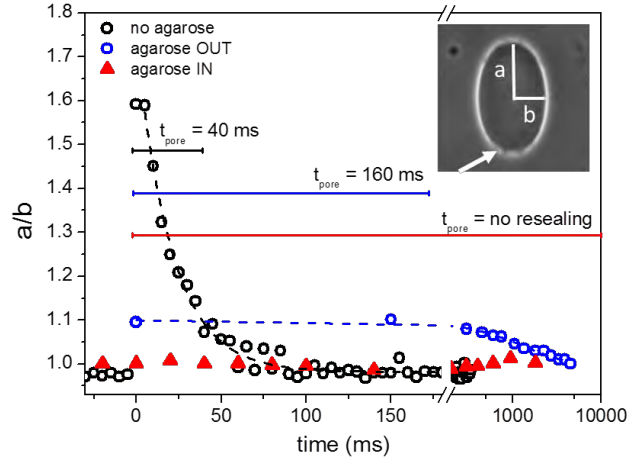


Figure S4. Vesicle aspect ratio a/b during electroporation for a GUV in agarose-free aqueous solution (open black circles), immobilized in agarose (open blue circles) and encapsulating agarose (solid red triangle). Dashed lines correspond to the fits using an exponential function with τ_{relax} as decay time. Horizontal lines indicate the period within which macropores are detected (corresponding to the pore lifetime t_{pore}). Inset shows maximal deformation of a GUV (aqueous solution) and its semi-axes a and b . The arrow points to the formed macropores.

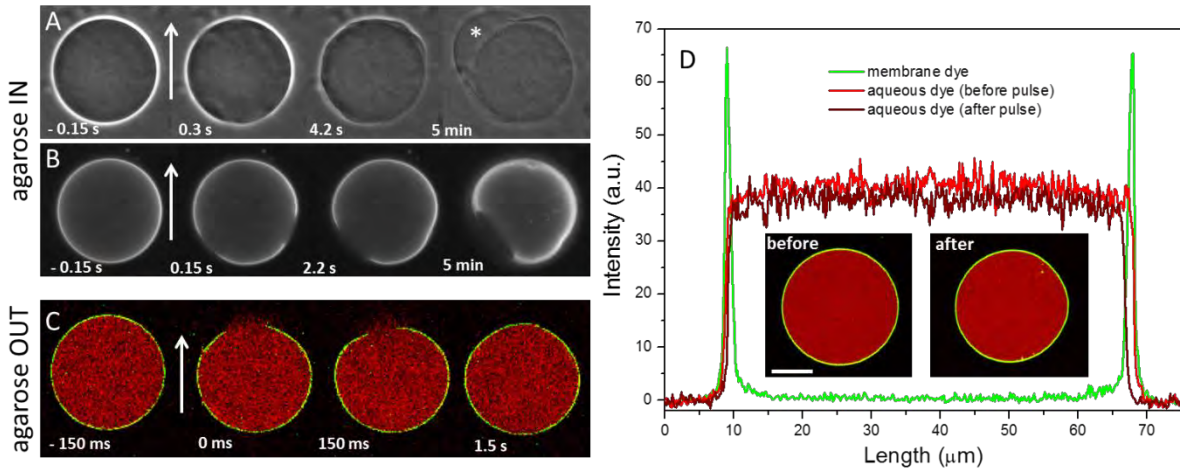


Figure S5. Effect of 0.5 % w/v agarose inside or outside GUVs exposed to electric pulses (3 kV/cm, 150 μ s). A), B) Sequences of two GUVs encapsulating agarose during application of a DC pulse, observed by phase contrast (A) and epifluorescence (B). The asterisk in A indicates the remaining GUV membrane. The spherical object next to it is the agarose mesh located inside the GUV before poration. The diameters of the initial GUVs in A and B are about 40 μ m. C) Confocal snapshots of a GUV dispersed in agarose and encapsulating 2.5 μ M sulforhodamine B before and after application of a DC pulse. The membrane is labeled with 0.5 mol% NBD-PE. Numbers correspond to time relative to the application of the pulse. The electric field direction is shown as an arrow. D) Fluorescence intensity of the membrane (green) and of sulforhodamine B (red) across the vesicle (same as in panel C and Figure 2C in the main text) before (light red) and 1 min after (dark red) pulse application, measured on the corresponding confocal images shown as insets. Bars: 20 μ m.

We next examined the response of immobilized GUVs (agarose only outside) to electric pulses. The vesicles contained encapsulated sulforhodamine B to allow detecting leakage through macropores and possibly long-lasting submicron pores, if present. As evidenced in Figure S5C, strong pulses lead to membrane poration (see interrupted membrane contour in green), and allow release of some of the encapsulated content. Analysis of the sulforhodamine B fluorescence intensity inside the GUV shows a 7% decrease after macropore resealing (see Figure S5D). Importantly, contrary to vesicles encapsulating agarose where residual agarose molecules block pore closure (Figures S5A and S5B, see also Ref. ²), the membrane here fully reseals and no long-term leakage is detected, suggesting that the agarose scaffold around the vesicle does not obstruct the membrane resealing even though increasing the pore lifetime ($t_{\text{pore}} \sim 160$ ms). The overall vesicle deformation is stronger than that of vesicles encapsulating agarose, but weaker than that of vesicles in agarose-free medium. This outcome is understandable considering the gel-like environment of the agarose-immobilized GUVs, which does not allow for the vesicles to freely deform. The relaxation time of the immobilized vesicles is also slower than that of agarose-free vesicles, $\tau_{\text{relax}} \sim 1.4$ s (Figure S4). This finding was reproducible for all vesicles analyzed, and observed for vesicles containing 50 or 100 mol% of POPG lipids (not shown). Apparently, the vesicle deformation induced by the pulse induces rearrangement of the agarose mesh around it, which in return slows down the relaxation of the deformed vesicle.

In summary, these results demonstrate a different behavior of GUVs subjected to mechanical strain when agarose is present in their interior or exterior. While GUV integrity is lost when agarose is present inside (Figures S5A and S5B), membrane integrity is maintained in immobilized vesicles (agarose outside, Figure S5C and S5D) and only their relaxation and pore lifetime are slowed down because of the presence of the external agarose scaffold. The results broadly validate the mechanical confinement provided by agarose and the preservation of vesicle structural integrity, allowing reliable measurements to be performed on agarose-immobilized GUVs.

S5. Diffusion of molecules to immobilized GUVs after gelation

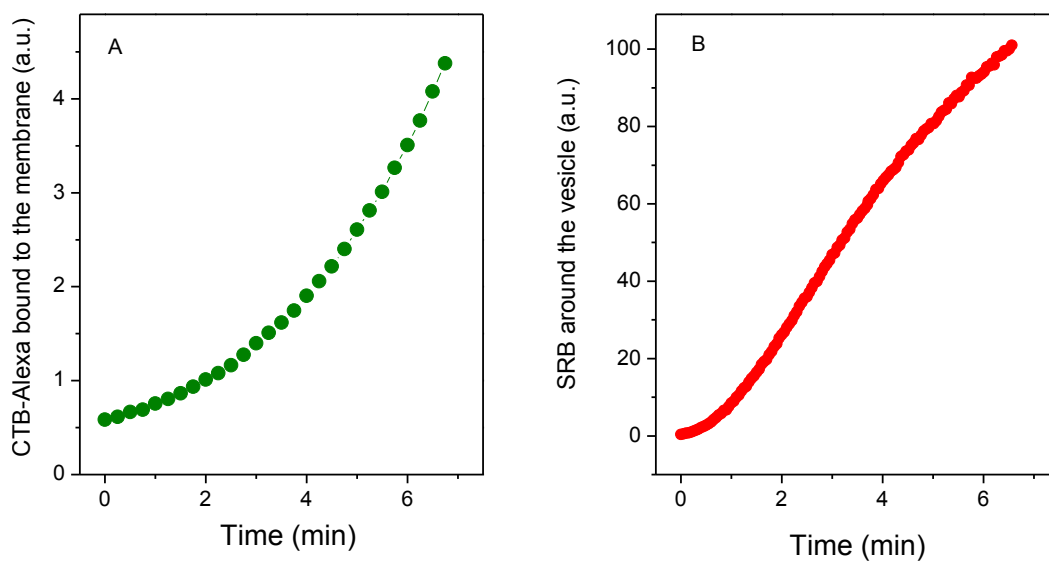


Figure S6. Time dependence of the fluorescence intensity of A) CTB-Alexa bound to the immobilized GUV and B) SRB around the GUV. The data were collected in the sequences shown in Figure 2B (A) and 2C (B) from the manuscript.

S6. Diffusion of aqueous probes in the agarose mesh measured with FCS and FRAP.

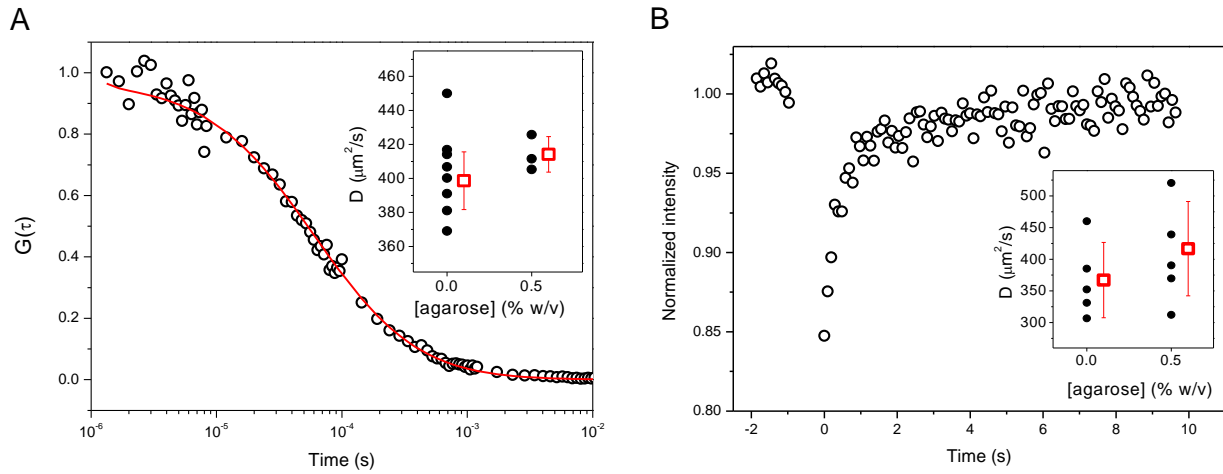


Figure S7. A) Representative normalized autocorrelation curve of 10 nM sulforhodamine B in solution (no agarose) with corresponding fit (red line). The inset shows diffusion coefficient values measured for SRB in solution with and without 0.5 % w/v agarose and the mean values with standard deviation. B) Representative FRAP recovery curve obtained for 0.2 μM carboxyfluorescein in the presence of 0.5 % w/v agarose. The photobleached area was large (20 μm diameter) to probe long-range diffusion as compared to FCS data which shows only short-range diffusion (within the confocal volume with dimensions of about $2 \times 0.3 \times 0.3 \mu\text{m}^3$). Details on the FRAP analysis are given in Figure S9. The inset shows diffusion coefficients measured for CF in solution with and without 0.5 w/v agarose and the mean values with standard deviation.

Table S1. Measured diffusion coefficient D (mean value \pm SD, $\mu\text{m}^2/\text{s}$) of DiI C18 (FCS) and NBD-PE (FRAP) in membranes of different lipid composition. The GUVs were immobilized in 0.5% w/v agarose.

	POPC	POPC:POPG 1:1	POPG
FCS	8.3 ± 1.8	6.4 ± 0.8	4.9 ± 0.4
FRAP	9.8 ± 1.7	8.3 ± 1.2	7.0 ± 1.0

S7. Mobility of liposomes in agarose.

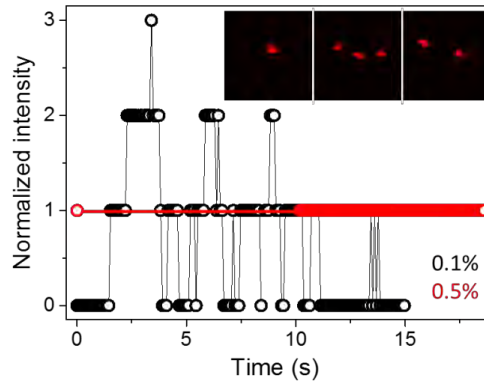


Figure S8. Quantification of liposome mobility for two agarose concentrations. The number of liposomes in a selected ROI (5 μm diameter) was counted over time and is plotted for the two agarose concentrations tested. The inset shows representative images of different number of liposomes in the ROI region imaged (5 μm x 5 μm) at 0.1% agarose. At 0.5% w/v agarose (red data), the single liposome imaged does not leave the ROI nor do other liposomes enter it.

S8. Determination of the effective radius of the bleached area

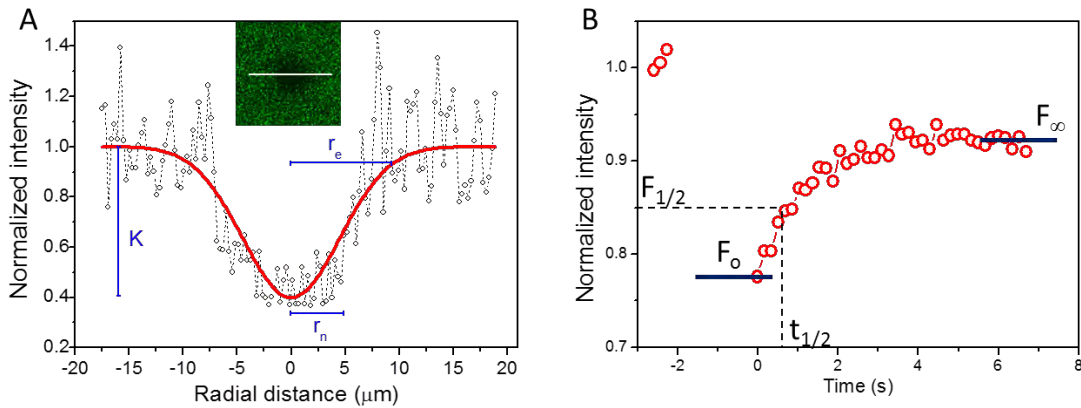


Figure S9. A) Measurement of the effective radius r_e . The intensity line profile of the first post-bleach spot is shown in black. The red line is the fit according to the equation $f(x) = 1 - K \exp\left(-\frac{2x^2}{r_e^2}\right)$ (eq. 2 in the main text and Ref. ⁴). The nominal radius ($r_n = 5 \mu\text{m}$), the effective radius ($r_e = 9 \mu\text{m}$) and the bleaching depth K are shown in blue. The inset shows the image used for the measurement. The effective radius was determined on bilayer patches on the cover slip surface, which resulted from GUVs that spontaneously ruptured and adhered to the glass surface in the presence of salts. This approach allowed better imaging of the bleached area. B) Typical FRAP recovery curve for a POPC GU immobilized in 0.5% (w/v) agarose. F_0 and F_∞ are the fluorescence intensities in the first post-bleach image and after recovery, respectively, and $t_{1/2}$ is the time to reach $F_{1/2} = (F_0 + F_\infty)/2$.

S9. Distribution of the number of Dil C18 molecules in the FCS volume.

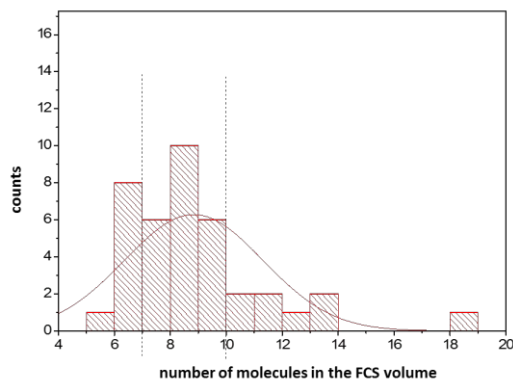


Figure S10. Histogram of the number of Dil C18 molecules in the FCS volume. The curve is a Gaussian fit of the data. Only measurements with dye concentration in the range between the dashed vertical lines were considered.

References

- 1 Horger, K. S., Estes, D. J., Capone, R. & Mayer, M. Films of Agarose Enable Rapid Formation of Giant Liposomes in Solutions of Physiologic Ionic Strength. *J. Am. Chem. Soc.* **131**, 1810-1819 (2009).
- 2 Lira, R. B., Dimova, R. & Rieke, K. A. Giant Unilamellar Vesicles Formed by Hybrid Films of Agarose and Lipids Display Altered Mechanical Properties. *Biophys. J.* **107**, 1609-1619 (2014).
- 3 Riske, K. A. & Dimova, R. Electro-deformation and poration of giant vesicles viewed with high temporal resolution. *Biophys. J.* **88**, 1143-1155 (2005).
- 4 Kang, M., Day, C. A., Kenworthy, A. K. & DiBenedetto, E. Simplified Equation to Extract Diffusion Coefficients from Confocal FRAP Data. *Traffic* **13**, 1589-1600 (2012).